ChemPhysChem

Research Article
doi.org/10.1002/cphc.202200396

Chemistry Europe
European Chemical Societies Publishing

www.chemphyschem.org

Thermally-Activated Tunneling in the Two-Water Bridge Catalyzed Tautomerization of Phosphinylidene Compounds**

Ashim Nandi*[a] and Jan M. L. Martin*[a]

Phosphinylidenes are an important class of organophosphorus compounds that can exhibit tautomerization between tricoordinated **P(III)** hydroxide (R^1R^2POH) and a pentacoordinated **P(V)** oxide ($R^1R^2P(O)H$) form. Herein we show, using the canonical variational transition state theory combined with multidimensional small-curvature tunneling approximation, the dominance of proton tunneling in the two-water-bridged tautomerizations of phosphinous acid and model phosphinylidenes comprising phosphosphinates, *H*-phosphonates, *H*-phosphinates and secondary phosphine oxides. Based on the studied system, the contribution of thermally-activated tunneling is predicted to speed up the semiclassical reaction rate by ca. threefold to as large as two orders of magnitude at 298.15 K in the gas phase. The large KIE and the concavity in the Arrhenius plots are further fingerprints of tunneling. The simulations also predicted that the rapid tunneling rate and short half-life span for the forward reaction, as opposed to the reverse reaction in fluorinated secondary phosphine oxides, would result in **P(V)** being elusive and only **P(III)** being isolable, which agrees with previous experiments where only **P(III)** was detected by IR and NMR spectroscopy. We also explored the role of solvent and predicted tunneling to be substantial.

Introduction

Phosphinylidenes are a family of organophosphorus compounds that are of biological and pharmaceutical importance.[1–3] They are also most commonly employed as ancillary ligands in homogenous catalysis.[4,5] These include phosphinates, *H*-phosphonates, *H*-phosphinates and secondary phosphine oxides. Such compounds can exhibit a prototropic (i.e., proton migration from one atom to another) tautomerism process involving structures with a tetracoordinate pentavalent phosphorus **P(V)** and a trivalent phosphorus **P(III)** atom (see Scheme 1A). Due to the availability of a free lone pair of electrons, the **P(III)** hydroxide form is known to coordinate with the metal in transition metal complexes. However, the **P(V)** oxide form is known to be the most stable species and the tautomeric equilibrium displayed in Scheme 1A is strongly shifted toward **P(V)** if the **R** were electron-donating groups. On the contrary, with electron-withdrawing fluororganyl groups, only the **P(III)** tautomer was isolated and detected spectroscopically, and in some cases, a solvent-dependent equilibrium was observed between the tautomeric forms.[6–10]

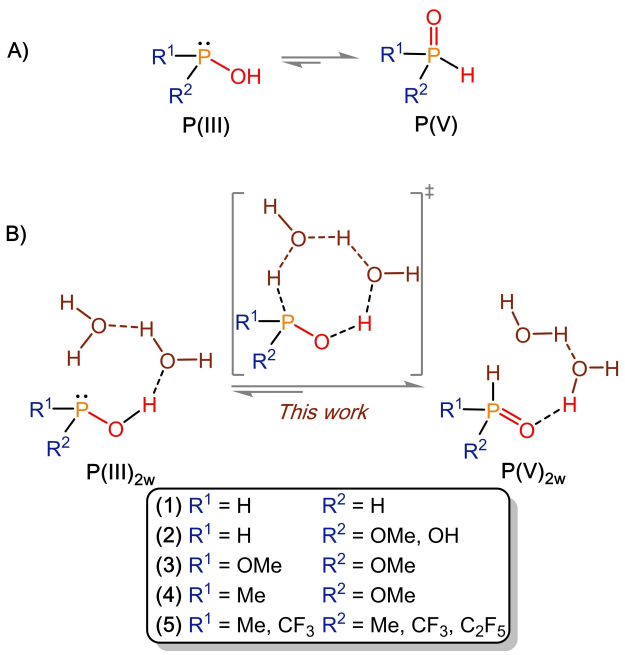

Scheme 1. Tautomerization reaction in phosphinylidene compounds showing **A)**. Intramolecular proton transfer (PT) and **B)**. Two water-bridged PT. R^1 and R^2 represent various substituents.

Although the reactivity of phosphinylidenes suggests the presence of both oxide and acid tautomers, the direct intramolecular proton transfer (PT) for their interconversion is unfavorable at room temperature due to its high activation barrier of ~60 kcal mol^{-1}.[11–15] Alternatively, an intermolecular PT mechanism between two tautomers of the same species,[16] a

[a] *Dr. A. Nandi, Prof. Dr. J. M. L. Martin*
Department of Molecular Chemistry and Materials Science
Weizmann Institute of Science
7610001 Rehovot, Israel
E-mail: ashim.nandi@weizmann.ac.il
gershom@weizmann.ac.il

[**] *A previous version of this manuscript has been deposited on a preprint server (https://doi.org/10.26434/chemrxiv-2022-0z4gm).*

Supporting information for this article is available on the WWW under https://doi.org/10.1002/cphc.202200396

base- or water-catalyzed PT has been proposed.[11,14,15,17] Recently, a detailed computational study on the tautomerization of simple secondary phosphine oxides predicted that the two-water bridged PT provides the most energetically favorable path in the gas phase, as compared to intra- and intermolecular PT involving one, two, or three tautomers.[12]

Due to its small mass, it is well-known that, for reactions with narrow barrier width, hydrogen can undergo quantum tunneling through the potential barrier.[18,19] Consequently, tunneling enhances the reaction rates and thereby lowers the measured activation energy.[20–24] The extent to which tunneling occurs in a chemical reaction[21,25] can be approximated as

$$P \sim e^{-w\sqrt{\Delta E^{\ddagger} m}/\hbar} \quad (1)$$

where P represents the probability of tunneling, w the barrier width, $\triangle E^{\ddagger}$ is the activation energy, m the reduced mass, and $\hbar$ the reduced Planck constant. Tautomerization plays a vital role in chemistry and biology and proton tunneling has been well-established in such processes.[22,26,27] Water as a catalyst in tautomerization reactions, and the influence of tunneling in them, have been documented. Examples include the important role of tunneling in the one- or two water-bridged tautomerization of formamidine[28,29] and azaindole,[30–32] keto-enol and amino-enol processes.[33–35] Furthermore, some of these cases validated experimental observations.[32–35] Using a one-dimensional tunneling approximation, tunneling has also been studied for the intermolecular tautomerization of the simplest phosphinous acid (H_2POH) and secondary phosphine oxides.[36–38] However, whether an accurate multidimensional tunneling method would find a tunneling mechanism to be viable has not been explored for the kinetically favored water-catalyzed tautomerization of phosphinylidenes. Since solvents, which stabilize the phosphinylidenes,[7,11,13] usually contain trace amounts of water, and considering the above sets of examples of water-assisted tunneling-driven tautomerism, studies to accurately assess the possibility of tunneling in the water-bridged tautomerization of phosphinylidenes are warranted.

In this article, we systematically investigate the two water-catalyzed tautomerizations of phosphinous acid (**1**) and phosphinylidenes substituted at the $\mathbf{R^1}$ and $\mathbf{R^2}$ positions, each representing a class of phosphinates (**2**), *H*-phosphonates (**3**), *H*-phosphinates (**4**) and secondary phosphine oxides (**5**) (see Scheme 1B). Using canonical variational transition state theory inclusive of multidimensional small-curvature tunneling, we shall demonstrate the significant tunneling contribution to the two-water bridged tautomerization process of **1–5** in the gas phase as well as in solvent media. The concave Arrhenius plots and abnormally high KIE reveal unambiguous fingerprints of tunneling at room temperature. We also explore the kinetics of reversibility of the experimentally reported fluorinated systems **5** and propose a possible reason for the elusive nature of **P(V)** tautomer.

Theoretical Method

To obtain accurate reaction rates with multidimensional tunneling corrections, it is crucial to correctly map the potential energy surface of the reaction. Hence, to select a reliable level of theory in terms of balance between accuracy and computational cost, we performed several DFT benchmark calculations on the activation energy ($\Delta E^{\ddagger}$) for the forward and reverse reaction for the two-water bridge tautomerization in $\mathbf{1_{H,H}}$ and $\mathbf{2_{H,OH}}$ using CCSD(T)[39] with the cc-pVQZ-F12 basis set.[40] (It has recently been shown[41] that this basis set,[40] while strictly speaking developed for explicitly correlated calculations, is also advantageous for orbital-only correlated wavefunction calculations.) In total, we assessed twelve different DFT functionals, namely, the GGA PBE;[42] the meta-GGA TPSS;[43] the three hybrid-GGAs PBE0,[44,45] TPPSh[43,46] and B3LYP,[47,48] with and without D3 correction;[49] five hybrid-meta-GGAs −B1B95,[50] PW6B95,[51] BMK[52] with and without D3 correction,[49] MN15,[53] and M06-2X,[54] and finally the long-range corrected hybrids wB97X[55] and wB97X-D,[56] all of these in conjunction with four triple-ζ quality basis sets (Def2-TZVP, 6–311 + G(d,p), aug-cc-pVTZ and cc-pVTZ). From the benchmark analysis, the BMK/Def2-TZVP combination emerged as the best performer, with a calculated barrier height $\Delta E^{\ddagger}$ within 1.0 kcal mol^{-1} of the CCSD(T)/cc-pVQZ-F12 reference (see Table S1 and S2 in the Supporting Information). Therefore, all molecular geometries, electronic energies, and their derivatives were computed at the BMK[52]/Def2-TZVP level using the *Gaussian 16* program system.[57] The CCSD(T) computations were performed using the MOLPRO2021 package.[58]

Semiclassical (without tunneling) reaction rates were computed using canonical variational transition state theory (CVT),[59] with tunneling contributions added within the small curvature tunneling (SCT) approximation.[60,61] In this study, we will refer to the CVT and SCT rate constants as k_{SC} and k_T. Polyrate17[62] was used to compute all the rate constants, with Gaussrate17[63] serving as the interface between Polyrate and Gaussian 16. A step size of 0.002 Bohr (with a scaling mass of 1 amu) was employed to map the reaction energy paths for all the reactions.[64] For hydrogen tunneling reactions with extremely narrow barrier width, the tunneling path may deviate far from the minimum energy path potential (V_{MEP}), following a straight line from reactant to product. In such scenarios, it is recommended to use the more accurate and computationally expensive large-curvature tunneling (LCT) method,[60,65] which follows a straight-line tunneling path, or a microcanonical optimized multidimensional tunneling (μOMT) approximation,[60,65] which estimates the optimal transmission probability as the greater of the SCT and LCT transmission probabilities at a given energy. Our benchmark analysis of SCT shows rates that are similar to those obtained using μOMT and slightly larger than LCT, indicating that the reaction path curvatures were not very large and thus safely confirming the suitability of our cost-effective SCT computations for our studied systems (see Supporting Information).

Results and Discussion

Tautomerization Mechanism

We first explored the possible mechanism of water-catalyzed tautomerization on $\mathbf{1_{H,H}}$ as a model compound (see Figure 1). In this and all the water-catalyzed reactions considered in this study, the reaction path was followed in the exergonic direction as was previously studied.[12,15,16] Table 1 presents the reaction and activation energies for the six different reaction pathways for transforming **P(III)**→**P(V)** and Figure 1 depicts their corre-

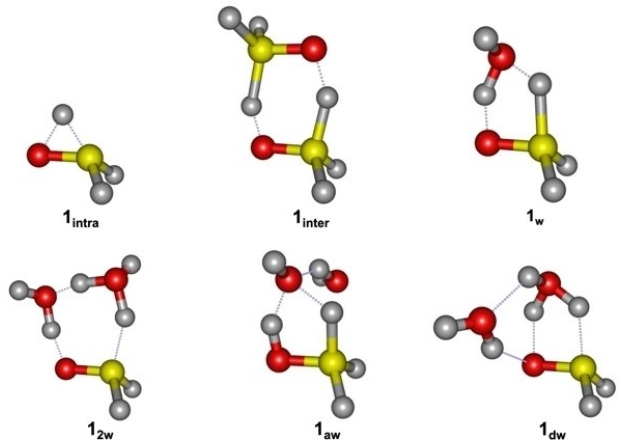

Figure 1. Transition state structures for the tautomerization in $\mathbf{1}_{H,H}$ involving water-unassisted intramolecular ($\mathbf{1}_{intra}$), intermolecular ($\mathbf{1}_{inter}$) dimer-assisted proton transfer (PT), one ($\mathbf{1}_{w}$) and two ($\mathbf{1}_{2w}$) water-assisted, and one water-assisted bonded to a second water molecule acting as a H-bond acceptor ($\mathbf{1}_{aw}$) and donor ($\mathbf{1}_{dw}$) in the PT.

Table 1. Threshold ($\triangle E^{\ddagger}$) and Gibbs free activation energies ($\triangle G^{\ddagger}$), along with their corresponding reaction energies ($\triangle E_r$) and reaction free energies ($\triangle G_r$) in kcal mol^{-1} for the intramolecular PT and various water-catalyzed tautomerization of $\mathbf{1}_{H,H}$. All the electronic energies include the zero-point energy corrections.

	$\triangle E^{\ddagger}$	$\triangle E_r$	$\triangle G^{\ddagger}$	$\triangle G_r$
$\mathbf{1}_{intra}$	64.1	−0.8	64.3	−0.5
$\mathbf{1}_{inter}$	31.3	−3.4	31.5	−2.0
$\mathbf{1}_{w}$	33.6	−0.7	35.6	−0.0
$\mathbf{1}_{2w}$	23.9	−0.9	26.0	−0.7
$\mathbf{1}_{aw}$	34.0	−1.6	36.7	−0.4
$\mathbf{1}_{dw}$	31.1	−7.4	32.4	−7.4

sponding transition state (TS) structures. In the absence of water, the intramolecular ($\mathbf{1}_{intra}$) direct proton transfer (PT) and the intermolecular ($\mathbf{1}_{inter}$) dimer-assisted PT are unfavorable for the reaction to occur at RT due to their high activation free energy barriers ($\triangle G^{\ddagger}$) of 64.3 and 31.5 kcal mol^{-1}, respectively, with the latter path resulting in an endothermic reaction. Moving to water-assisted PT, we computed the reaction pathway with one ($\mathbf{1}_{w}$) and two bridging water molecules ($\mathbf{1}_{2w}$). In addition, we also studied the reaction with the bridging water bonded to a second water acting as a hydrogen bond donor ($\mathbf{1}_{dw}$) and acceptor ($\mathbf{1}_{aw}$), as a prototype to study the influence of a water-wire mechanism on the $\triangle G^{\ddagger}$ (see Figure 1). As shown in Table 1, the $\triangle G^{\ddagger}$ values for the one-water bridged pathways $\mathbf{1}_{w}$, $\mathbf{1}_{dw}$ and $\mathbf{1}_{aw}$ are in the range of 29.8–34.0 kcal mol^{-1}, too high for the reaction to happen at room temperature. This is attributed to the highly strained three-membered ring at the TS. The $\triangle G^{\ddagger}$ for the two-water bridged $\mathbf{1}_{2w}$ pathway has the lowest barrier (26.0 kcal mol^{-1}); albeit slightly high for a RT reaction in the absence of tunneling, we will see the latter's influence below. The $\triangle G^{\ddagger}$ lowering for $\mathbf{1}_{2w}$ stems from the relaxed seven-membered ring TS, which makes it efficient for the PT instead of the sterically hindered TS adopted in the above cases. Similar mechanistic analysis on $\mathbf{2}_{H,OH}$ also revealed the same trend in the activation barriers and reaction energies, giving the lowest activation free barrier (22.6 kcal mol^{-1}) with two-water assisted PT (see Table S3 in the Supporting Information). The detailed analysis of these reaction mechanisms suggests that the two-water assisted PT is the most kinetically preferred path, consistent with previous study predicted for other phosphinylidenes.[12] Therefore, calculations on all the tautomerization reactions considered in this study were carried out with the two-water bridge acting as a mediator for the PT.

Table 2 lists the computed barriers, reaction energies and the characteristics imaginary frequency of the transition state for all the studied systems, namely phosphinous acid ($\mathbf{1}_{H,H}$), phosphinates ($\mathbf{2}_{H,OH}$ and $\mathbf{2}_{H,OMe}$), *H*-phosphonates ($\mathbf{3}_{Ome,Ome}$), *H*-phosphinates ($\mathbf{4}_{Me,Ome}$) and secondary phosphine oxides ($\mathbf{5}_{CF3,CF3}$ and $\mathbf{5}_{CF3,C2F5}$) (Scheme 1B). It can be seen that, except for $\mathbf{1}_{H,H}$, the computed free energy barriers for **1**–**5** are well below 25.0 kcal mol^{-1}, suggesting that the reaction is favorable under experimental conditions. Notably, in the absence of water, the intramolecular tautomerization process in all these cases yields prohibitively high barriers of 52–64 kcal mol^{-1}, rendering the reaction forbidden at RT (see Table S4 in the Supporting Information). For the electron-donating substituted systems **1**–**4**, the reaction is exothermic in the direction of the $\mathbf{P(V)}_{2w}$ oxide form. In contrast, for the electron-withdrawing groups (entries 7 and 8 in Table 2), the acid $\mathbf{P(III)}_{2w}$ hydroxide form is more stable, consistent with prior studies mentioned above.

Table 2. Threshold ($\triangle E^{\ddagger}$) and Gibbs free activation energies ($\triangle G^{\ddagger}$), along with their corresponding reaction energies ($\triangle E_r$) and reaction free energies ($\triangle G_r$) in kcal mol^{-1}, and transition state imaginary frequencies (ν) in cm^{-1} for the two-water bridged tautomerization of **1**–**5** systems. All the energies include the zero-point energy corrections.

	$\triangle E^{\ddagger}$	$\triangle E_r$	$\triangle G^{\ddagger}$	$\triangle G_r$	ν
$\mathbf{1}_{H,H}$	23.9	−0.9	26.0	−0.7	−1386
$\mathbf{2}_{H,OMe}$	22.8	−9.3	24.7	−9.3	−1410
$\mathbf{2}_{H,OH}$	20.7	−17.6	22.6	−17.0	−1468
$\mathbf{3}_{OMe,OMe}$	19.3	−13.1	21.3	−13.6	−1414
$\mathbf{4}_{Me,OMe}$	19.4	−11.5	21.5	−11.8	−1592
$\mathbf{5}_{Me,Me}$	20.0	−9.0	22.1	−9.0	−1664
$\mathbf{5}_{CF3,CF3}$ [a]	17.3	−5.7	17.6	−7.2	−527
$\mathbf{5}_{CF3,C2F5}$ [a]	15.8	−6.9	18.6	−5.9	−482

[a] The tautomerization reaction was studied from $\mathbf{P(V)}_{2w} \rightarrow \mathbf{P(III)}_{2w}$.

Quantum Tunneling Rates

As discussed above, tunneling is known to play a dominant role in several tautomerization reactions. We therefore ventured to explore the tunneling rates in the two water-catalyzed tautomerizations of **1**–**5** systems. Except for $\mathbf{1}_{H,H}$, our computed semiclassical k_{SC} rates show that the reaction should be feasible under experimental conditions at 298.15 K (see Table 3). However, as discussed below, the assistance of tunneling is predicted to significantly accelerate the reaction rates for all the studied systems.

Considering first the simplest case of phosphinous acid $\mathbf{1}_{H,H}$, the contribution of the tunneling transmission coefficient (κ_T) is predicted to be the largest among all the studied reactions, giving a κ_T value of 138 at 298.15 K. Such a sizable tunneling effect is probably the largest hitherto predicted for a tautomerization reaction at room temperature. This kappa factor results in an apparent reaction barrier ~3.0 kcal mol^{-1} below the classical barrier height at 298.15 K, indicative of tunneling from thermally activated states rather than the ground-state vibrational level ($v=0$).[22] It is interesting to note that for $\mathbf{1}_{H,H}$, the semiclassical k_{SC} rate of 5×10^{-7} s^{-1} yield a $t_{1/2}$ (calculated as ln(2)/k) of 16 days, which is too slow for the reaction to occur under standard experimental conditions; however, inclusion of tunneling results in a k_T of 7×10^{-5} and a corresponding $t_{1/2}$ of ~3 hrs, thus leading to an experimentally observable rate at 298.15 K: considering its short half-life, if the hydroxide form of $\mathbf{1}_{H,H}$ were prepared by some methods in the gas phase at RT, then its tunneling decay rate to its oxide form should be able to be monitored by spectroscopic methods, e.g., IR or NMR.

Moving to the phosphonates (**2**), inclusion of tunneling also reveals a large enhancement of the semiclassical rate by factors of 124 and 115 for $\mathbf{2}_{H,OMe}$ and $\mathbf{2}_{H,OH}$ at 298.15 K, respectively. For $\mathbf{3}_{OMe,OMe}$, $\mathbf{4}_{Me,OMe}$ and $\mathbf{5}_{Me,Me}$, the tunneling effect results in a κ_T of 77, 60 and 43 at 298.15 K, indicating that 98–99% of the reaction rates for the above cases are due to tunneling. In the case of $\mathbf{5}_{CF3,CF3}$ and $\mathbf{5}_{CF3,C2F5}$, tunneling accelerates their semiclassical rate by ~3 times, although small compared to the above phosphinylidenes, still accounting for 63 to 65% to the overall reaction rate.

Furthermore, the consequences of tunneling in **1**–**5** can also be seen from the Arrhenius graph (see Figure 2 for six selected systems), for which the k_T rates (solid curves) show a distinct concave curve diverging from the semiclassical k_{SC} rates (dotted straight line) and not reaching a flat plateau as the temperature decreases, which is an indication of a reaction assisted by thermally-activated tunneling. The Arrhenius graph conspicuously reveals that as the temperature is lowered, the contribution of the tunneling grows, reaching a κ_T on the order of ~10^3–10^4 for all the above systems at 225 K, making the reaction possible even when the classical over-the-barrier process is forbidden (see Supporting Information for rates table). As the temperature increases beyond 298.15 K, the contribution of tunneling, albeit lowered as thermal reaction begins to dominate at these temperatures, is still substantial, speeding up the semiclassical k_{SC} rates by 1.4 to 8 times faster at 400 K.

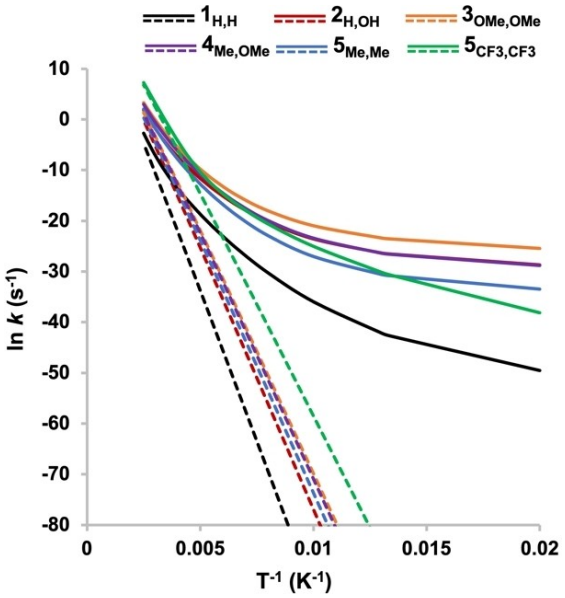

Figure 2. Arrhenius plot for the rate constants without (k_{sc}, dotted lines) and with tunneling corrections (k_T, solid lines) for a temperature range of 50 to 400 K for **1**–**5**.

We now turned our attention to investigating the kinetic reversibility of the experimentally reported tautomerization of fluorinated systems (**5**). Previous gas-phase experimental study on $\mathbf{5}_{CF3,CF3}$ and $\mathbf{5}_{CF3,C2F5}$ revealed only the exclusive presence of the **P(III)** form by IR and NMR spectroscopy.[66] To understand this observation, we analyzed the kinetic reversibility of their

Table 3. Semiclassical rate constants without (k_{SC}) and with tunneling correction (k_T) in s^{-1}, tunneling transmission coefficient (κ_T), tunneling corrected half-life ($t_{1/2}$) in s, and %tunneling contribution for the bridged tautomerization reactions involving systems **1**–**5** at 298.15 K.

	k_{SC}	k_T	κ_T	$t_{1/2}$	%tunneling[b]
$1_{H,H}$	5×10^{-7}	7×10^{-5}	138	10^4	99
$2_{H,OMe}$	5×10^{-6}	6×10^{-4}	124	10^3	99
$2_{H,OH}$	2×10^{-4}	2×10^{-2}	115	34	99
$3_{OMe,OMe}$	2×10^{-3}	0.1	77	6	99
$4_{Me,OMe}$	10^{-3}	7×10^{-2}	60	10	98
$5_{Me,Me}$	4×10^{-4}	2×10^{-2}	43	39	98
$5_{CF3,CF3}$[a]	0.6	2	2.8	0.3	65
$5_{CF3,C2F5}$[a]	0.1	0.3	2.7	2	63

[a] The tautomerization reaction was studied from $\mathbf{P(V)}_{2w}\rightarrow\mathbf{P(III)}_{2w}$. [b] % tunneling $=1-(k_{SC}/k_T)$.

reaction by comparing the tunneling rate constants and their half-life time for the reverse reaction, i.e., $\mathbf{P(III)_{2w}}\rightarrow\mathbf{P(V)_{2w}}$ to those of the corresponding forward rates $\mathbf{P(V)_{2w}}\rightarrow\mathbf{P(III)_{2w}}$. Noteworthy, the ratio between **P(III)** and **P(V)** concentration will depend on the energy difference between the tautomers.[66] Still, we can explain this ratio from the relationship of the kinetic rate constants and their corresponding half-lives. Since the reverse reaction is endergonic, we obtained their rates through scaling the rate constants calculated in the exergonic direction by their microscopic reversibility.[67] For $\mathbf{5_{CF3,CF3}}$, the reverse rate constants yield a k_T of 1×10^{-4} s^{-1} at 298.15 K. This corresponds to a tunneling-corrected $t_{1/2}$ of 1.4 hrs. On the other hand, the rapid tunneling rate k_T of 2 s^{-1} for the forward reaction implies a $t_{1/2}$ of only 0.3 s, suggesting that the **P(V)** oxide tautomer is too short-lived a species and that only the **P(III)** form should be detected under normal experimental conditions at RT, in agreement with the aforementioned experimental observation.

Similarly, in the case of $\mathbf{5_{CF3,C2F5}}$, the computed reverse rate constant results in a k_T of 3×10^{-6} s^{-1} with a tunneling $t_{1/2}$ of 20 hrs versus k_T of 0.3 s^{-1} and $t_{1/2}$ of ~2 s calculated for the forward reaction at 298.15 K, indicating the ephemeral character of **P(V)** oxide tautomer and thereby, this might explain the reason why only the **P(III)** form is present in the reported NMR spectra.

It is also worth mentioning that for electron-donating systems $\mathbf{2_{H,OMe}}$, $\mathbf{2_{H,OH}}$, $\mathbf{3_{OMe,OMe}}$ and $\mathbf{4_{Me,OMe}}$, their high exergonicity of the reaction and extremely facile tunneling rates would correspond to extremely short half-lives ranging between 10^3 and 6 s (See Table 1) thereby making the reaction $\mathbf{P(III)_{2w}}\rightarrow\mathbf{P(V)_{2w}}$ irreversible. Therefore, while the tunneling decay rate for $\mathbf{2_{H,OMe}}$ ($t_{1/2}$ of 19 min.) might be amenable to experimental study, the hydroxide $\mathbf{P(III)_{2w}}$ species will be fleeting and only the oxide $\mathbf{P(V)_{2w}}$ form would be isolated and detected experimentally. Therefore, this prediction on our model systems might explain the possible reason why the phosphinylidenes with electron donor substituted group prefers to exist in oxide form, as mentioned above.

Influence of Barrier Width on the kappa Factor

To rationalize the trend in the tunneling contribution, a comparison of barrier height and width is instructive. An apparent observation in the tunneling transmission coefficient for **1**–**5** shows that κ_T decreases with decreasing barrier height. This might suggest that lower barriers in these systems are associated with broader barrier widths, thereby lowering the κ_T values. Since the imaginary vibrational frequency (ν) of a TS can dictate the topology in the vicinity of the TS and is a measure of the curvature of the reaction coordinate at the TS, it might be expected that a larger barrier height would correspond to a larger imaginary frequency for the reaction coordinate, and in turn to a thinner barrier. However, for our studied reactions, there is no clear correlation between barrier height and TS imaginary frequency. For instance, in $\mathbf{1_{H,H}}$ the TS has a ν of -1386 cm^{-1} and a $\triangle G^{\neq}$ of 26.0 kcal mol^{-1}, whereas $\mathbf{5_{Me,Me}}$ the one with a large ν of -1664 cm^{-1}, has a $\triangle G^{\neq}$ of 22.1 kcal mol^{-1}.

Closer scrutiny of the TS structures of **1**–**5** shows that a shorter (longer) bond length of the P(**O**–**H**) bond corresponds to a larger (smaller) imaginary frequency, giving a Badger type correlation.[68,69] For instance, the P(**O**–**H**) bond at the TS for $\mathbf{5_{Me,Me}}$ with the largest ν has the shortest bond length of 1.226 Å, whereas $\mathbf{5_{CF3,C2F5}}$ with the smallest ν has the longest bond length of 1.619 Å, respectively. Overall, we observed an absolute linear variation between υ and P(**O**–**H**) bond length for our studied systems ($R^2=0.99$; see Figure 3).

Figure 4 shows the potential energy curves of the minimum energy path (V_{mep} in solid curve) and the vibrationally adiabatic ground-state energy curves (V_a^G in dotted curve), which include the zero-point energies along the mass-scaled reaction coor-

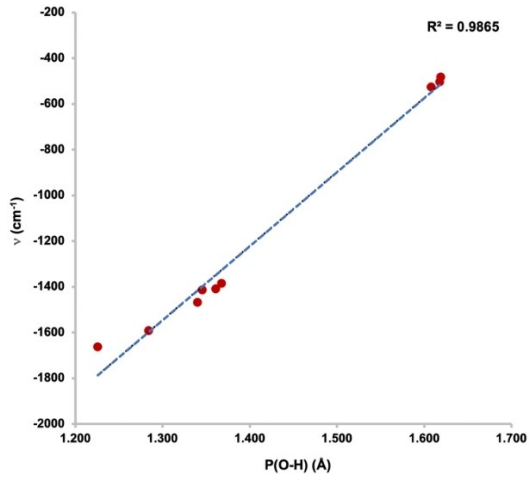

Figure 3. Plot of imaginary frequency (ν) in cm^{-1} of the transition states versus P(**O**–**H**) bond length in Å for systems **1**–**5**.

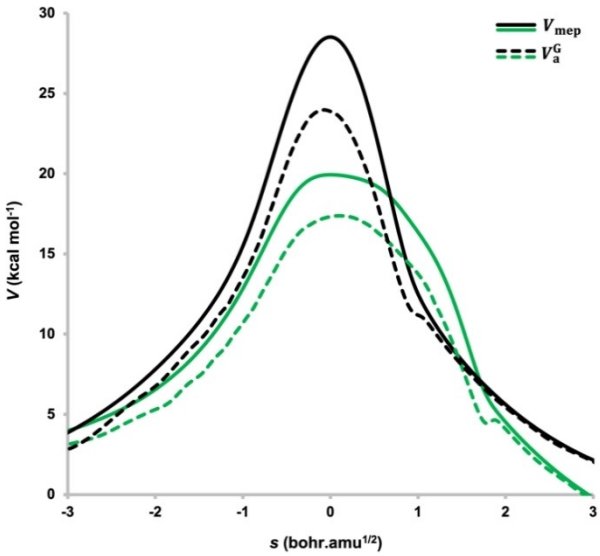

Figure 4. Potential (V_{mep}) and adiabatic ground-state energy (V_a^G) curves along the mass-scaled reaction coordinate (s) for two water-bridged tautomerization of $\mathbf{1_{H,H}}$ (in black curves) and $\mathbf{5_{CF3,CF3}}$ (green curves).

dinate (*s*) for two extreme cases i.e., $\mathbf{1}_{H,H}$ and $\mathbf{5}_{CF3,CF3}$. First, from the plots, it can be seen that no stable intermediates were observed in the potential and adiabatic energy curves along the reaction coordinate, which indicates that the three hydrogens in the two-water bridged tautomerization were transferred concertedly. Second and most interestingly, the broadness (round top and flatten section) of the V_{mep} and V_a^G curve around the TS region is evident for $\mathbf{5}_{CF3,CF3}$ as compared to $\mathbf{1}_{H,H}$, which exhibit a higher but narrow barrier shape ideal for swift tunneling. This observation thus indicates that a high barrier possesses a more sharply rising or narrow potential and adiabatic energy curves, resulting in an expected large κ_T.

Kinetic Isotope Effects and Fingerprint for Tunneling

The most common diagnostic tool to check for the evidence of tunneling in chemical reactions has been the measurement of kinetic isotope effects (KIEs). For a thermal reaction, replacing hydrogen in the broken or formed C–H bond with deuterium typically leads to a decrease in the reaction rates with KIE (k_H/k_D) of ~7 at 298.15 K.[26] For KIEs beyond this semiclassical limit, it is generally realized that the reaction is driven by tunneling.[22,70] We therefore studied the KIE, to test the tunneling effect, by taking $\mathbf{1}_{H,H}$ and $\mathbf{2}_{H,OH}$ as a model compound. Since the bond-breaking and bond-formation during the tautomerization involve significant movement of three hydrogens (H_1, H_2 and H_3), as reflected in the eigenvectors corresponding to the TS imaginary frequency (see Figure 5), we checked the KIE(k_{H1H2H3}/k_{D1D2D3}) and predicted a dramatically large tunneling-corrected KIE_T of 500.1 for $\mathbf{1}_{H,H}$ and 465.7 for $\mathbf{2}_{H,OH}$ at 298.15 K, giving a strong indication of proton tunneling in this systems. We further studied the KIEs of these hydrogens separately to dissect their individual contributions and find the "tunneling-determining atom"[71] i.e., the atom that has the greatest influence on the tunneling rates. Figure 5 shows the labeled atoms with their calculated KIEs with and without tunneling corrections. The semiclassical KIE_{SC} for all the hydrogens is below 5 at 298.15 K, whereas incorporating tunneling enhances the KIE_T resulting in a value of 6.2, 6.0 and 31.0 for H_1, H_2 and H_3, the latter value showing strong evidence of tunneling. A similar trend in the KIE_T was also predicted for $\mathbf{2}_{H,OH}$, giving a maximum value of 19.6 for H_3 (see Figure 5).

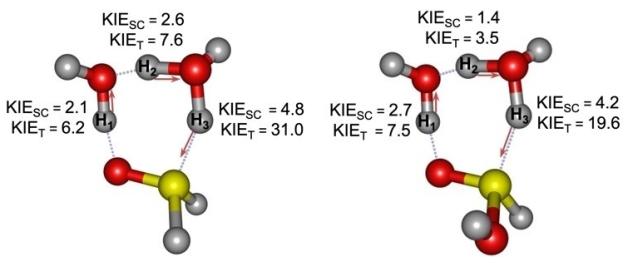

Figure 5. Computed kinetic isotope effect (k_H/k_D) without (KIE_{sc}) and with the inclusion of tunneling (KIE_T) for the labeled atoms at 298.15 K. The arrows depicts the eigen vectors of the water-catalyzed PT at the TS for $\mathbf{1}_{H,H}$, and $\mathbf{2}_{H,OH}$.

These results indicate that the hydrogen (H_3) making a bond with the phosphorous atom is the tunneling-determining atom. Therefore, our computational prediction of tunneling can in principle be validated by measuring the KIE of the P–H(D) bond.

Effect of Solvents on the Tunneling Rates

As mentioned above, it has been shown that the presence of solvents of varying polarity has a significant influence on the stability of the phosphinylidene tautomers as well as on the activation barriers and reaction energies of its tautomerization.[7,8,12] For multidimensional tunneling computations, the use of explicit solvent in the reaction is alas computationally intractable. To study the solvent effect on the tunneling rates, we computed the rate constants using an implicit polarizable continuum model,[72] which can at least *mimic* the role of the electrostatic effect on the tunneling rates. We studied the reaction with the highest kappa factor, i.e., $\mathbf{1}_{H,H}$ and along with two other systems $\mathbf{5}_{Me,Me}$ and $\mathbf{5}_{CF3,CF3}$ in three different solvents, namely toluene ($\varepsilon = 2.4$), THF ($\varepsilon = 7.4$) and water ($\varepsilon = 78.4$). $\mathbf{5}_{Me,Me}$ and $\mathbf{5}_{CF3,CF3}$ were selected for the sake of comparing the nature of electron-donating and -withdrawing groups on the tunneling rates in solvent media.

An obvious observation from Table 4 is that the reaction becomes more exothermic along with slightly lower $\triangle G^{\neq}$, resulting in faster reaction rates as we move from gas phase to increase the polarity of the solvents. This might be explained through stabilization of the TS and the product state via stronger electrostatic interaction with a highly polar solvent.

Analyzing the κ_T factor in solvent media shows that the tunneling is substantial and that its contribution decreases going from the gas phase to increasingly polar solvents for $\mathbf{1}_{H,H}$ and $\mathbf{5}_{CF3,CF3}$, with the latter approaching a semiclassical value of ~1, indicating that the thermal reaction dominates due to lower barriers. In the case of $\mathbf{5}_{Me,Me}$, however, there is no clear trend, with κ_T being higher in toluene than in the gas phase, and an intermediate value in THF. This may not be the case when the

Table 4. Solvent dielectric constant (ε), activation free energy ($\triangle G^{\neq}$) and reaction energy ($\triangle G_r$) in kcal mol^{-1}, semiclassical (k_{SC}) and tunneling rate constant (k_T) in s^{-1}, tunneling transmission coefficient (κ_T), for $\mathbf{1}_{H,H}$, $\mathbf{5}_{Me,Me}$ and $\mathbf{5}_{CF3,CF3}$[a] in the gas phase and four solvents at 298.15 K.

	medium	ε	$\triangle G^{\neq}$	$\triangle G_r$	k_{SC}	k_T	κ_T
$1_{H,H}$	gas	1.0	26.0	−0.7	5×10^{-7}	7×10^{-5}	138
	toluene	2.4	25.4	−1.3	10^{-6}	10^{-4}	90
	THF	7.4	24.9	−3.6	3×10^{-6}	2×10^{-4}	63
	water	78.4	24.6	−2.6	6×10^{-6}	3×10^{-4}	47
$5_{Me,Me}$	gas	1.0	22.1	−9.0	4×10^{-4}	2×10^{-2}	43
	toluene	2.4	20.9	−10.1	2×10^{-3}	0.3	112
	THF	7.4	20.5	−14.0	5×10^{-3}	0.5	105
	water	78.4	20.3	−13.7	8×10^{-3}	0.3	42
$5_{CF3,CF3}$	gas	1.0	17.6	−7.2	0.6	2	3
	toluene	2.4	14.0	−8.3	40	70	1.8
	THF	7.4	11.6	−9.2	10^3	2×10^3	1.1
	water	78.4	13.4	−8.7	4×10^2	5×10^2	1.3

[a] The tautomerization reaction was studied from $\mathbf{P(V)}_{2w}\rightarrow\mathbf{P(III)}_{2w}$.

reaction is carried out in a real solvent, since the presence of solvent would increase the effective mass of the transferring proton via interaction with the surrounding solvent dipoles, which in turn would reduce the tunneling contribution according to the tunneling probability (*P*) expression in Eq. 1.

Conclusions

In summary, we have examined the two-water catalyzed tautomerization of phosphinous acid (**1**) and model phosphinylidene compounds, each serving as representative cased of phosphinates (**2**), *H*-phosphonates (**3**), *H*-phosphinates (**4**) and secondary phosphine oxides (**5**). Depending on the systems, our rate constant calculations, including the multidimensional small-curvature tunneling approximation, show that tunneling significantly accelerates the gas-phase semiclassical reaction rates by ca. threefold to as large as two orders of magnitude at 298.15 K. The predicted unusually high KIE (k_H/k_D), and the concave Arrhenius graph of the tunneling rate constants around the room temperature regime, while not reaching a flat plateau as the temperature is lowered further, reveals the dominance of proton tunneling and its occurrence from the vibrational excited level by a thermally-activated tunneling process. We have also shown that for fluorinated secondary phosphine oxides, the rapid tunneling rate and short half-life time for the forward $\mathbf{P(V)_{2w}}\rightarrow\mathbf{P(III)_{2w}}$ reaction results in the fleeting existence of the **P(V)** tautomer, thus explaining the possible reason why only the **P(III)** form was previously detected by IR and NMR spectroscopy. Furthermore, we tested the influence of solvent (using a polarized continuum model) on the tunneling rates and predicted an influential role of tunneling for the systems with electron-donating groups **1**–**4**. In contrast, due to low barriers, the semiclassical over-the barrier process becomes dominant for fluorinated systems **5** in a highly polar solvent. The present computational study thus elucidates the influential role of the tunneling effect in a family of model phosphinylidenes, thereby making it into the gallery of water-assisted tautomerization processes driven exclusively *via* a tunneling mechanism.

Acknowledgements

This research was supported by the Israel Science Foundation (grant 1969/20) and by the Minerva Foundation (grant 2020/05). A.N. acknowledge the Feinberg Graduate School of the Weizmann Institute of Science for the Dean's Excellence Postdoctoral Fellowship. We would like to thank Prof. Sebastian Kozuch for bringing the topic of phosphinylidenes to our attention.

Conflict of Interest

The authors declare no conflict of interest.

Data Availability Statement

The data that support the findings of this study are available in the supplementary material of this article.

Keywords: hydrogen tunneling · computational chemistry · tautomerism · phosphine oxides · kinetic isotope effects

[1] L. D. Quin, *A Guide to Organophosphorus Chemistry*, John Wiley & Sons, **2000**.
[2] D. E. C. Corbridge, *Phosphorus: Chemistry, Biochemistry and Technology, Sixth Edition*, CRC Press, **2013**.
[3] J.-L. Montchamp, *Acc. Chem. Res.* **2014**, *47*, 77–87.
[4] R. H. Crabtree, *The Organometallic Chemistry of Transition Metals*, Wiley, Hoboken, NJ, **2009**.
[5] A. Börner, *Phosphorus Ligands in Asymmetric Catalysis: Synthesis and Applications*, WILEY-VCH, Weinheim, **2008**.
[6] J. E. Griffiths, A. B. Burg, *J. Am. Chem. Soc.* **1962**, *84*, 3442–3450.
[7] B. Kurscheid, W. Wiebe, B. Neumann, H.-G. Stammler, B. Hoge, *Eur. J. Inorg. Chem.* **2011**, *2011*, 5523–5529.
[8] A. Christiansen, C. Li, M. Garland, D. Selent, R. Ludwig, A. Spannenberg, W. Baumann, R. Franke, A. Börner, *Eur. J. Inorg. Chem.* **2010**, *2010*, 2733–2741.
[9] B. Hoge, J. Bader, H. Beckers, Y. S. Kim, R. Eujen, H. Willner, N. Ignatiev, *Chem. Eur. J.* **2009**, *15*, 3567–3576.
[10] J. Stawinski, A. Kraszewski, *Acc. Chem. Res.* **2002**, *35*, 952–960.
[11] B. G. Janesko, H. C. Fisher, M. J. Bridle, J.-L. Montchamp, *J. Org. Chem.* **2015**, *80*, 10025–10032.
[12] D. Vincze, P. Ábrányi-Balogh, P. Bagi, G. Keglevich, *Molecules* **2019**, *24*, 3859.
[13] G. Manca, M. Caporali, A. Ienco, M. Peruzzini, C. Mealli, *J. Organomet. Chem.* **2014**, *760*, 177–185.
[14] S. S. Wesolowski, N. R. Brinkmann, E. F. Valeev, H. F. Schaefer, M. P. Repasky, W. L. Jorgensen, *J. Chem. Phys.* **2002**, *116*, 112–122.
[15] D. B. Chesnut, *Heteroat. Chem.* **2000**, *11*, 73.
[16] Y. V. Babin, A. V. Prisyazhnyuk, Y. A. Ustynyuk, *Russ. J. Phys. Chem.* **2008**, *82*, 94–100.
[17] K. D. Troev, in *Reactivity of P-H Group of Phosphorus Based Compounds* (Ed.: K. D. Troev), Academic Press, **2018**, pp. 1–17.
[18] R. P. Bell, *The Tunneling Effect in Chemistry*, Chapman And Hall, London, **1980**.
[19] P. R. Schreiner, *Trends Chem.* **2020**, *2*, 980–989.
[20] W. T. Borden, *WIREs Comput. Mol. Sci.* **2016**, *6*, 20–46.
[21] J. Meisner, J. Kästner, *Angew. Chem. Int. Ed.* **2016**, *55*, 5400–5413; *Angew. Chem.* **2016**, *128*, 5488–5502.
[22] E. M. Greer, K. Kwon, A. Greer, C. Doubleday, *Tetrahedron* **2016**, *72*, 7357–7373.
[23] S. Kozuch, T. Schleif, A. Karton, *Phys. Chem. Chem. Phys.* **2021**, *23*, 10888–10898.
[24] C. Castro, W. L. Karney, *Angew. Chem. Int. Ed.* **2020**, *59*, 8355–8366; *Angew. Chem.* **2020**, *132*, 8431–8442.
[25] A. Nandi, S. Kozuch, J. Kästner, *Chem. Phys. Lett.* **2020**, *754*, 137678.
[26] J. P. Layfield, S. Hammes-Schiffer, *Chem. Rev.* **2014**, *114*, 3466–3494.
[27] Z. D. Nagel, J. P. Klinman, *Chem. Rev.* **2006**, *106*, 3095–3118.
[28] R. L. Bell, D. L. Taveras, T. N. Truong, J. Simons, *Int. J. Quantum Chem.* **1997**, *63*, 861–874.
[29] R. L. Bell, T. N. Truong, *J. Chem. Phys.* **1994**, *101*, 10442–10451.
[30] M. P. T. Duong, K. Park, Y. Kim, *J. Photochem. Photobiol. A* **2010**, *214*, 100–107.
[31] H. Fang, Y. Kim, *J. Chem. Theory Comput.* **2013**, *9*, 3557–3566.
[32] A. Fernández-Ramos, Z. Smedarchina, W. Siebrand, M. Z. Zgierski, M. A. Rios, *J. Am. Chem. Soc.* **1999**, *121*, 6280–6289.
[33] B. K. Mai, K. Park, M. P. T. Duong, Y. Kim, *J. Phys. Chem. B* **2013**, *117*, 307–315.
[34] T. Kaweetirawatt, T. Yamaguchi, T. Higashiyama, M. Sumimoto, K. Hori, *J. Phys. Org. Chem.* **2012**, *25*, 1097–1104.
[35] P. C. Sam, B. Carlos, R. Tokmakoff, *PNAS* **2013**, *110*, 9243–9248.
[36] A. V. Prisyazhnyuk, Y. V. Babin, *J. Struct. Chem.* **2005**, *46*, 164–167.
[37] V. M. Mamaev, A. V. Prisyajnuk, D. N. Laikov, L. S. Logutenko, Y. V. Babin, *Mendeleev Commun.* **1999**, *9*, 240–241.
[38] H. Tavakol, F. Keshavarzipour, *Heteroat. Chem.* **2016**, *27*, 210–220.

[39] K. Raghavachari, G. W. Trucks, J. A. Pople, M. Head-Gordon, *Chem. Phys. Lett.* **1989**, *157*, 479–483.
[40] K. A. Peterson, T. B. Adler, H.-J. Werner, *J. Chem. Phys.* **2008**, *128*, 084102.
[41] H. Kruse, R. Szabla, J. Šponer, *J. Chem. Phys.* **2020**, *152*, 214104.
[42] J. P. Perdew, K. Burke, M. Ernzerhof, *Phys. Rev. Lett.* **1996**, *77*, 3865–3868.
[43] J. Tao, J. P. Perdew, V. N. Staroverov, G. E. Scuseria, *Phys. Rev. Lett.* **2003**, *91*, 146401.
[44] C. Adamo, V. Barone, *J. Chem. Phys.* **1999**, *110*, 6158–6170.
[45] M. Ernzerhof, G. E. Scuseria, *J. Chem. Phys.* **1999**, *110*, 5029–5036.
[46] V. N. Staroverov, G. E. Scuseria, J. Tao, J. P. Perdew, *J. Chem. Phys.* **2003**, *119*, 12129–12137.
[47] A. D. Becke, *Phys. Rev. A* **1988**, *38*, 3098–3100.
[48] C. Lee, W. Yang, R. G. Parr, *Phys. Rev. B* **1988**, *37*, 785–789.
[49] S. Grimme, J. Antony, S. Ehrlich, H. Krieg, *J. Chem. Phys.* **2010**, *132*, 154104.
[50] A. D. Becke, *J. Chem. Phys.* **1996**, *104*, 1040–1046.
[51] Y. Zhao, D. G. Truhlar, *J. Phys. Chem. A* **2005**, *109*, 5656–5667.
[52] A. D. Boese, J. M. L. Martin, *J. Chem. Phys.* **2004**, *121*, 3405–3416.
[53] H. S. Yu, X. He, S. L. Li, D. G. Truhlar, *Chem. Sci.* **2016**, *7*, 5032–5051.
[54] Y. Zhao, D. G. Truhlar, *Theor. Chem. Acc.* **2008**, *120*, 215–241.
[55] J.-D. Chai, M. Head-Gordon, *J. Chem. Phys.* **2008**, *128*, 084106.
[56] J.-D. Chai, M. Head-Gordon, *Phys. Chem. Chem. Phys.* **2008**, *10*, 6615–6620.
[57] *Gaussian 16, Rev. C.01*, M. J. Frisch, G. W. Trucks, H. B. Schlegel, G. E. Scuseria, M. A. Robb, J. R. Cheeseman, G. Scalmani, V. Barone, G. A. Petersson, H. Nakatsuji, X. Li, M. Caricato, A. V. Marenich, J. Bloino, B. G. Janesko, R. Gomperts, B. Mennucci, H. P. Hratchian, J. V. Ortiz, A. F. Izmaylov, J. L. Sonnenberg, D. Williams-Young, F. Ding, F. Lipparini, F. Egidi, J. Goings, B. Peng, A. Petrone, T. Henderson, D. Ranasinghe, V. G. Zakrzewski, J. Gao, N. Rega, G. Zheng, W. Liang, M. Hada, M. Ehara, K. Toyota, R. Fukuda, J. Hasegawa, M. Ishida, T. Nakajima, Y. Honda, O. Kitao, H. Nakai, T. Vreven, K. Throssell, J. A. Montgomery, Jr., J. E. Peralta, F. Ogliaro, M. J. Bearpark, J. J. Heyd, E. N. Brothers, K. N. Kudin, V. N. Staroverov, T. A. Keith, R. Kobayashi, J. Normand, K. Raghavachari, A. P. Rendell, J. C. Burant, S. S. Iyengar, J. Tomasi, M. Cossi, J. M. Millam, M. Klene, C. Adamo, R. Cammi, J. W. Ochterski, R. L. Martin, K. Morokuma, O. Farkas, J. B. Foresman, D. J. Fox, Gaussian, Inc., Wallingford, CT **2019**.
[58] H.-J. Werner, P. J. Knowles, F. R. Manby, J. A. Black, K. Doll, A. Heßelmann, D. Kats, A. Köhn, T. Korona, D. A. Kreplin, Q. Ma, T. F. Miller, A. Mitrushchenkov, K. A. Peterson, I. Polyak, G. Rauhut, M. Sibaev, *J. Chem. Phys.* **2020**, *152*, 144107.
[59] D. G. Truhlar, B. C. Garrett, *Annu. Rev. Phys. Chem.* **1984**, *35*, 159–189.
[60] A. Fernandez-Ramos, B. A. Ellingson, B. C. Garrett, D. G. Truhlar, in *Rev. Comput. Chem.*, Wiley-Blackwell, **2007**, pp. 125–232.
[61] R. T. Skodje, D. G. Truhlar, B. C. Garrett, *J. Chem. Phys.* **1982**, *77*, 5955–5976.
[62] *POLYRATE-version 2017*, J. Zheng, J. L. Bao, R. Meana-Pañeda, S. Zhang, B. J. Lynch, J. C. Corchado, Y.-Y. Chuang, P. L. Fast, W.-P. Hu, Y.-P. Liu, G. C. Lynch, K. A. Nguyen, C. F. Jackels, A. Fernandez Ramos, B. A. Ellingson, V. S. Melissas, J. Villà, I. Rossi, E. L. Coitiño, J. Pu, T. V. Albu, A. Ratkiewicz, R. Steckler, B. C. Garrett, A. D. Isaacson, D. G. Truhlar, University of Minnesota, Minneapolis, MN, **2017**.
[63] *GAUSSRATE 17-B*, J. Zheng, J. L. Bao, S. Zhang, J. C. Corchado, R. Meana-Pañeda, Y.-Y. Chuang, E. L. Coitiño, B. A. Ellingson, D. G. Truhlar, University of Minnesota, Minneapolis, MN, **2017**.
[64] M. Page, J. W. McIver, *J. Chem. Phys.* **1988**, *88*, 922–935.
[65] J. L. Bao, D. G. Truhlar, *Chem. Soc. Rev.* **2017**, *46*, 7548–7596.
[66] N. Allefeld, M. Grasse, N. Ignat'ev, B. Hoge, *Chem. Eur. J.* **2014**, *20*, 8615–8620.
[67] S. Karmakar, A. Datta, *J. Phys. Chem. B* **2016**, *120*, 945–950.
[68] R. M. Badger, *J. Chem. Phys.* **1934**, *2*, 128–131.
[69] M. A. Boyer, O. Marsalek, J. P. Heindel, T. E. Markland, A. B. McCoy, S. S. Xantheas, *J. Phys. Chem. Lett.* **2019**, *10*, 918–924.
[70] Y. Kim, M. M. Kreevoy, *J. Am. Chem. Soc.* **1992**, *114*, 7116–7123.
[71] S. Kozuch, *Phys. Chem. Chem. Phys.* **2014**, *16*, 7718–7727.
[72] J. Tomasi, B. Mennucci, R. Cammi, *Chem. Rev.* **2005**, *105*, 2999–3093.

Revised manuscript received: July 15, 2022
Accepted manuscript online: July 22, 2022
Version of record online: August 18, 2022